Paleoclimates, 1997, Vol. 2(1), pp. 71–99
Reprints available directly from the publisher
Photocopying permitted by license only

SENSITIVITY OF THE THERMOHALINE CIRCULATION FOR DIFFERENT CLIMATES — INVESTIGATIONS WITH A SIMPLE ATMOSPHERE-OCEAN MODEL

MATTHIAS PRANGE,[a] GERRIT LOHMANN,[b,*] and RÜDIGER GERDES[a]

[a]*Alfred-Wegener-Institute for Polar and Marine Research, Am Handelshafen 12, D-27570 Bremerhaven, and* [b]*Max-Planck-Institute for Meteorology, Bundesstr. 55, D-20146 Hamburg, Germany*

(Received 15 September 1996; In final form 19 March 1997)

Palaeoclimatic records indicate several abrupt changes in North Atlantic climate which are assumed to be caused by disturbances of the thermohaline circulation (THC). By means of an idealized ocean box model we investigate the sensitivity of the THC with respect to a high-latitudinal salinity reduction, simulating a sudden meltwater release of glaciers or icebergs. We study the influence of various surface heat and freshwater flux parameterization schemes. By coupling an atmospheric energy balance model to the ocean model the importance of atmospheric heat and moisture transports in destabilizing the THC is demonstrated.

Furthermore, the THC and its sensitivity under different climatic conditions is investigated. Due to the temperature-dependence of the thermal expansion coefficient the oceanic circulation weakens and becomes more vulnerable with decreasing global temperatures. The results indicate that during Ice Ages even relatively weak freshwater invasions might have caused considerable variations in the intensity of the THC, accompanied by severe cold snaps in high latitudes due to the weakened oceanic heat transport.

Keywords: Thermohaline circulation, box models, atmospheric transports, palaeoceanography

INTRODUCTION

Greenland ice cores and other climate records clearly indicate that various abrupt changes in the North Atlantic climate occured in the past. A well documented event is the Younger Dryas (11,000 years B.P.), the last millennium-long cold period, whose marks can be found from Canada to Scandinavia. It is presumed

*Corresponding author.

that those changes are connected with freshwater invasions into the North Atlantic, resulting in a weakening of the thermohaline-driven ocean circulation (THC) and consequently in a decreased oceanic poleward heat transport (Broecker, 1991). Palaeoclimatic studies actually show relations between meltwater events owing to retreating glaciers (Keigwin *et al.*, 1991) or massive discharges of icebergs launched from Canada (Bond, 1995; Bond *et al.*, 1992) and cold snaps in the North Atlantic region. The cooling in high latitudes strengthens the THC again, whereas the decrease in poleward influx of salty water tends to amplify the initial perturbation.

Atmospheric responses to oceanic temperature anomalies play an essential role in stabilizing or destabilizing the THC after a freshwater perturbation. These responses are reflected in enhanced poleward eddy heat and moisture transports due to an increased mean meridional air temperature gradient and hence intensified baroclinicity. For numerical model studies this means that the parameterization of surface heat and freshwater fluxes fundamentally affects the sensitivity of the large-scale model circulation. However, numerous previous model studies employ rather unphysical *ad hoc* formulations for surface fluxes in order to simplify the coupled climate system. Mixed boundary conditions (i.e. the combination of a temperature restoring condition with a fixed freshwater flux at the oceanic surface) are used in the studies of (among others) Bryan (1986), Weaver and Hughes (1994), and Weaver *et al.* (1994). Zhang *et al.* (1993) employ the heat flux formulation of Schopf (1983) (fixed horizontal atmospheric heat transports and surface freshwater fluxes) in their sensitivity studies. Stocker *et al.* (1992) as well as Rahmstorf and Willebrand (1995) derive thermal boundary conditions based on atmospheric energy balance. Nakamura *et al.* (1994) and Lohmann *et al.* (1996a) extend the energy balance by including atmospheric moisture transports. The studies of Zhang *et al.* (1993), Rahmstorf and Willebrand (1995) and Lohmann *et al.* (1996a) show that mixed boundary conditions highly overestimate the THC's sensitivity, whereas Schopf's formulation results in an exaggerated stability.

In the present work we couple an oceanic box model with an atmospheric EBM, including variable air temperatures and eddy heat and moisture transports. A box model provides a qualitative understanding of thermohaline feedback mechanisms with relatively low computational expenditure and is a common tool for THC stability and variability studies (*e.g.*, Nakamura *et al.*, 1994; Lohmann *et al.*, 1996b; Tang and Weaver, 1995). The atmospheric EBM works with physical approximations of governing processes where the transport terms are parameterized as diffusion. By certain simplifications of the atmospheric model component we can reproduce various surface heat and freshwater flux formulations. By a comparative study we will see how the simplifications affect the sensitivity of the present-day equilibrium state with regard to freshwater perturbations. Additionally, the

effect of a simple temperature-albedo feedback will be investigated to take into account the high albedoes of snow and ice which form when high-latitudinal temperatures drop.

For a deeper understanding of climate variability and sensitivity, studies on the THC's stability in climates which differ from the current one are necessary. In the present work we will generate different climatic states by altering the energy balance at the top of the atmosphere. We will investigate the stability of the resulting equilibrium states. To the authors' knowledge, up to now there are no stability investigations of the large-scale ocean circulation in a coupled mode in colder or warmer climates than the current one, although it is evident that the stability of the THC strongly depends on the background state on which it operates.

The paper is organized as follows: In section 1 we describe the coupled box model. Stability investigations with regard to various surface flux parameterizations are presented and discussed in section 2. In section 3 the stability of the THC in different climates is studied. Discussions and interpretations of the results follow. Conclusions are drawn in section 4.

1. MODEL DESCRIPTION

Ocean Model

We consider a one-hemisphere ocean basin which reaches meridionally from 10°*N* to 70°*N* and is 80° in width to represent crudely the North Atlantic (Fig. 1). The ocean is subdivided into three boxes. The upper ocean is represented by a low-latitude and a high-latitude box (box 1 and box 2, respectively), separated at 45°*N* and coupled by heat and freshwater fluxes with the overlying atmosphere. The model is completed by a deep ocean box 3. The ocean boxes are coupled advectively to each other, and a sinking in high latitudes is considered, so that the prognostic equations for the temperatures T_i and salinities S_i of the three boxes ($i = 1, 2, 3$) read:

$$\frac{dT_1}{dt} = \frac{q}{V_1}(T_3 - T_1) + \frac{F_{oa,1}}{\rho c_p \Delta z}, \tag{1}$$

$$\frac{dT_2}{dt} = \frac{q}{V_2}(T_1 - T_2) + \frac{F_{oa,2}}{\rho c_p \Delta z}, \tag{2}$$

$$\frac{dT_3}{dt} = \frac{q}{V_3}(T_2 - T_3), \tag{3}$$

$$\frac{dS_1}{dt} = \frac{q}{V_1}(S_3 - S_1) - \frac{S_0}{\Delta z} A_1 (P - E)_1, \tag{4}$$

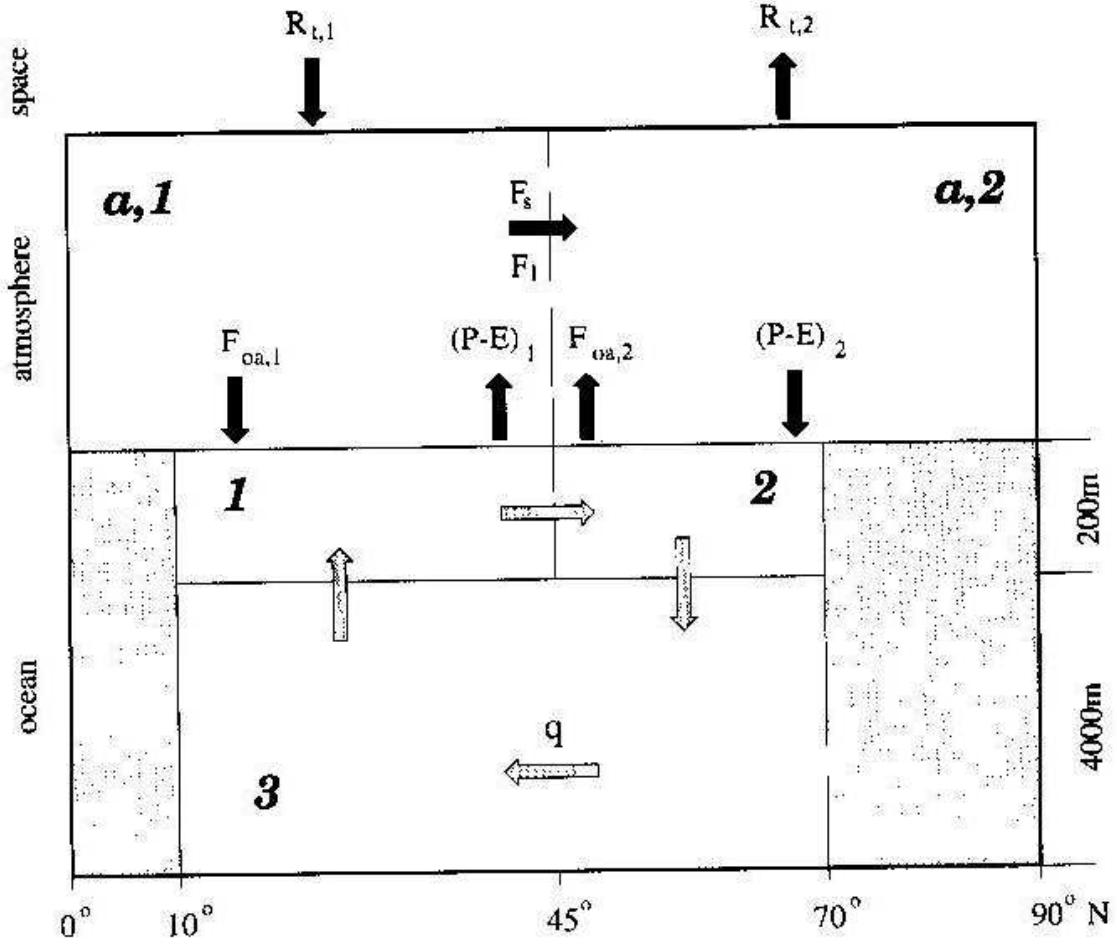

FIGURE 1 Schematic diagram of the coupled ocean-atmosphere model. The system's dynamic is driven by different energy balances $R_{t,i}$ at the top of the atmosphere. Poleward fluxes of sensible and latent heat (water vapour) F_s and F_l, respectively, arise in the atmosphere, while heat and salt is transported in the ocean by the THC with an overturning rate q. Ocean and atmosphere are coupled through heat and freshwater fluxes $F_{oa,i}$ and $(P-E)_i$, respectively.

$$\frac{dS_2}{dt} = \frac{q}{V_2}(S_1 - S_2) - \frac{S_0}{\Delta z} A_l (P-E)_2, \tag{5}$$

$$\frac{dS_3}{dt} = \frac{q}{V_3}(S_2 - S_3), \tag{6}$$

where $F_{oa}1$ and $F_{oa}2$ denote the surface heat fluxes for the low-latitude and the high-latitude box, respectively, and V_i the volumes of the three ocean boxes. S_0 is a reference salinity (35 *psu*), ρ a reference density (1025 $kg\ m^{-3}$), and c_p the specific heat of water (4200 $Jkg^{-1}{}^{\circ}C^{-1}$). The depth Δz of the upper ocean amounts to 200 *m*. $A_l(P-E)_1$ and $A_l(P-E)_2$ denote the surface freshwater fluxes (precipitation minus evaporation) out of the low- and into the high-latitude box, respectively. The multiplicative constant A_l is introduced to take account of the large

caption area of the North Atlantic ocean. The overturning rate q, *i.e.*, the volume flux of the THC between two adjacent ocean boxes, is assumed to depend on the square of the density difference between box 1 and 2:

$$q = c\,[\rho_{o,2}(T_2, S_2) - \rho_{o,1}(T_1, S_1)]^2, \tag{7}$$

where the densities (in $kg\ m^{-3}$) are calculated by a non-linear equation of state (Zhang *et al.*, 1993):

$$\rho_{o,i}(T_i, S_i) = 1003.0 + 0.77\,S_i - 0.072T_i(1 + 0.72T_i). \tag{8}$$

The factor c in (7) is freely tunable to adjust the strength of the thermohaline-driven overturning. The square law dependence on the density gradient of q can be derived from vorticity equations (Maas, 1994). Neither convection nor diffusion is included in the model.

Atmospheric Energy Balance Model

The ocean is coupled with an atmospheric EBM similar to the one described by Chen *et al.* (1995). In the present box model the atmosphere is subdivided into a low- and a high-latitude cell which zonally span the whole circumference of the globe (Figure 1). Assuming that both the sensible and the latent meridional heat fluxes vanish at the equator and at the pole, the following prognostic equations determine the surface air temperatures T_a,1 and T_a,2 of the low- and the high-latitude atmospheric cell, respectively:

$$\beta c_{p,a}\frac{dT_{a,1}}{dt} = -\frac{1}{2\pi a^2(\sin 45° - \sin 0°)}(F_s + F_l) + R_{t,1} - f_1 F_{oa,1}, \tag{9}$$

$$\beta c_{p,a}\frac{dT_{a,2}}{dt} = \frac{1}{2\pi a^2(\sin 90° - \sin 45°)}(F_s + F_l) + R_{t,2} - f_2 F_{oa,2}, \tag{10}$$

where $c_{p,a}$ denotes the specific heat of air ($1004\ Jkg^{-1}{}^{\circ}C^{-1}$), a the earth's radius ($6.37 \cdot 10^6\ m$), F_s and F_l the fluxes of sensible and latent heat from the southern to the northern atmospheric cell across the $45°N$ latitude circle, and $R_{t,i}$ the radiation balance at the top of the atmospheric cells. Since the ocean surface occupies only a fraction of the total hemispheric earth surface, the factors f_1 and f_2 are introduced. The factor $\beta c_{p,a}$ determines the time scale of atmospheric responses to thermal forcings. Chen *et al.* (1995) found $\beta = 5300\ kg\ m^{-2}$. The radiation balance at the top of the atmosphere $R_{t,i}$ is expressed by

$$R_{t,i} = R_{sol,i}(1 - \alpha_{p,i}) - I_i, \tag{11}$$

where $R_{sol,i}$ denotes the extraterrestrial solar insolation. The planetary albedo $\alpha_{p,i}$ is parameterized as a function of air temperature (Griffel and Drazin, 1981):

$$\alpha_{p,i} = 0.42 - 0.2 \tanh[0.052(T_{a,i} - 3.0)]. \tag{12}$$

The outgoing infrared radiation I_i is formulated by a linear dependence on surface air temperature (Budyko, 1969):

$$I_i = A + BT_{a,i}. \tag{13}$$

Chen *et al.* (1995) found the empirical constants A and B to be 213.35 $W\,m^{-2}$ and 2.22 $W\,m^{-2}{}^{\circ}C^{-1}$, respectively. Since atmospheric transports across the 45°N latitude circle are mainly due to transient eddies (Oort and Peixoto, 1983), F_s and F_l can be parameterized in terms of the meridional surface air temperature gradient, basing on linear baroclinic stability theory (Branscome, 1983; Stone and Yao, 1990):

$$F_s = K_s \left| \frac{\partial T_a}{a \partial \phi} \right|^n, \tag{14}$$

$$F_l = K_l r_h \left(\frac{\partial q_s}{\partial T_a} \right)_{T_a(45^{\circ}N)} \left| \frac{\partial T_a}{a \partial \phi} \right|^n, \tag{15}$$

where q_s denotes the temperature-dependent saturation specific humidity (see below) and $r_h = 0.8$ fixed relative humidity. The coefficients K_s and K_l are tuned to reproduce observational values of Michaud and Derome (1991). For the power n theoretical considerations (*e.g.*, Lohmann, 1995) as well as empirical studies (Stone and Miller, 1980) suggest $n = 2$. Approach (15) assumes that fluctuations in relative humidity are small compared to variations in specific humidity. The merit of this formulation is the plain relation to atmospheric temperatures. Alternatively, water vapour can be treated as a conservative variable, introducing a new transport equation (*e.g.*, Vallis, 1982; Fanning and Weaver, 1996).

To determine the temperature at 45°N we follow Nakamura *et al.* (1994) and assume that the latitudinal profile of the zonal mean surface air temperature can be approximated by the second Legendre Polynomial, and that T_a,1 and T_a,2 represent the zonal mean surface air temperatures at 20°N and 55°N, respectively. The corresponding meridional surface air temperature gradient at 45°N then reads:

$$\frac{\partial T_a}{a\partial\phi}(45°N) = \frac{1}{a[\sin^2(20°) - \sin^2(55°)]}(T_{a,1} - T_{a,2}). \tag{16}$$

Coupling of Ocean and Atmosphere

Assuming that net freshwater fluxes across the $10°N$ and the $70°N$ latitude circle vanish, the coupling of atmosphere and ocean through surface freshwater fluxes is calculated diagnostically by

$$(P-E)_1 = -\frac{1}{L_v\rho_w}\frac{1}{2\pi a^2(\sin 45° - \sin 10°)}F_f, \tag{17}$$

$$(P-E)_2 = \frac{1}{L_v\rho_w}\frac{1}{2\pi a^2(\sin 70° - \sin 45°)}F_f, \tag{18}$$

where L_v denotes the latent heat of vaporization ($2.5 \cdot 10^6\ J\ kg^{-1}$) and ρ_w the density of freshwater.

The net surface heat flux consists of the sum of shortwave radiation, net longwave radiation, latent and sensible heat exchanges:

$$F_{oa,i} = Q_{sw,i} - Q_{lw,i} - Q_{lh,i} - Q_{sh,i}. \tag{19}$$

Values for the shortwave radiation are prescribed basing on data given by Oberhuber (1988) ($Q_{sw},1 = 190\ W\ m^{-2}$, $Q_{sw},2 = 85\ W\ m^{-2}$). The net longwave radiation is parameterized by (*e.g.*, Isemer and Hasse, 1987; Hasse, 1993)

$$\begin{aligned} Q_{lw,i} = {} & C_{lw,i}(0.254 - 3.96\cdot 10^{-3} e_{s,i})(T_{a,i} + 273.15)^4 \\ & + 2.2\cdot 10^{-7}(T_{a,i} + 273.15)^3(T_i - T_{a,i}), \end{aligned} \tag{20}$$

with $C_{lw,1} = 4.0 \cdot 10^{-8} W\ m^{-2}°C^{-4}$ and $C_{lw,2} = 2.2 \cdot 10^{-8} W\ m^{-2}°C^{-4}$. The formulation of the temperature-dependent saturation water vapour pressure $e_{s,i}$ (in *mbar*) is taken from Shuttleworth (1993) and reads:

$$e_{s,i} = 6.11\exp\left(\frac{17.27\ T_{a,i}}{237.0 + T_{a,i}}\right). \tag{21}$$

Latent and sensible surface heat fluxes are parameterized similar as in Haney (1971) by

$$Q_{lh,i} = C_{lh,i}q_{s,i}(1 - r_h) + C_{lh,i}\left(\frac{\partial q_{s,i}}{\partial T_{a,i}}\right)(T_i - T_{a,i}), \tag{22}$$

$$Q_{sh,i} = C_{sh,i}(T_i - T_{a,i}). \tag{23}$$

Values given by Isemer and Hasse (1987) indicate $C_{lh,1} = 24600\ W\,m^{-2}$, $C_{lh,2} = 60900\ W\,m^{-2}$, $C_{sh,1} = 5\ W\,m^{-2}{}^{\circ}C^{-1}$, and $C_{sh,2} = 20\ W\,m^{-2}{}^{\circ}C^{-1}$ for the present box model. The saturation specific humidity $q_{s,i}$ is calculated by (*e.g.*, Haney, 1971)

$$q_{s,i}(T_{a,i}) = \frac{0.622}{1000\ mbar} e_{s,i}(T_{a,i}). \tag{24}$$

Integration of the system of coupled ordinary differential equations for the following stability studies is performed by an adaptive-step 5th-order Runge-Kutta scheme.

2. SURFACE FLUX PARAMETERIZATIONS

Results

The coupled box model is tuned to reproduce the current climate. The tuning parameters required are listed in Table I, and the obtained climatological values are shown in Table II. From (3) directly follows that $T_2 = T_3$ in equilibrium states. The current mode of the THC is characterized by a high-latitude sinking equilibrium with strong northward transports of heat and salt in the upper ocean layers. This equilibrium state is perturbed by an initial salinity reduction in the high-latitude ocean box 2, simulating a sudden meltwater release. For the present coupled system a salinity reduction of at least $S_2' = 1.35\ psu$ entails a breakdown of the current mode of the THC within one century. The new equilibrium state has no deep

TABLE I Tuning Parameters Employed for the Coupled Ocean-Atmosphere Model

Parameter	*Units*	*Value*
c	$[m^9 s^{-1} kg^{-2}]$	$4.3 \cdot 10^5$
K_s	$[W m^n {}^{\circ}C^{-n}]$	$\frac{6.5 \cdot 10^{25}}{(6.676 \cdot 10^{-6})^{n-2}}$
K_l	$[W m^n {}^{\circ}C^{-n+1}]$	$\frac{9.3 \cdot 10^{28}}{(6.676 \cdot 10^{-6})^{n-2}}$
$R_{sol,1}$	$[W m^{-2}]$	400.5
$R_{sol,2}$	$[W m^{-2}]$	261.3
A_t		2.1

TABLE II Features of Three Equilibrium States Describing Different Climates

Variable	*Units*	*Present Climate*	*Colder Climate*	*Warmer Climate*
T_1	[°C]	26.06	24.73	27.14
$T_2 = T_3$	[°C]	2.90	0.11	4.93
T_{a1}	[°C]	25.17	23.52	26.46
T_{a2}	[°C]	1.61	−1.31	3.83
S_1	[*psu*]	36.45	36.81	36.36
$S_2 = S_3$	[*psu*]	34.90	34.89	34.94
q	[*Sv*]	6.71	5.16	7.58
oceanic heat transport	[*PW*]	0.67	0.55	0.73
atmospheric heat transports:				
sensible F_s	[*PW*]	2.90	3.22	2.67
latent F_l	[*PW*]	1.59	1.52	1.65
total	[*PW*]	5.16	5.29	5.05
$A_1(P-E)_2$	[*cm/yr*]	71.19	67.92	73.60
F_{oa1}	[W/m^2]	22.17	18.09	24.04
F_{oa2}	[W/m^2]	−50.84	−41.49	−55.14
α_{p1}	[%]	25.63	26.23	25.21
α_{p2}	[%]	43.44	46.41	41.14

The stability of the THC in the present-day climate (left column) is studied in section 2 of the present paper. In section 3 the sensitivities of the THC in the colder and in the warmer climates are investigated.

water formation in high latitudes and is not modelled here (we refer to Stommel (1961) and Willebrand (1993) for further information on it). For smaller disturbances the THC can recover. The effect of a salinity reduction slightly smaller than S'_2 is presented in Figures 2–6. Figure 4,c shows the time series of the overturning rate q. Due to the meltwater perturbation it is instantaneously reduced to less than 4 *Sv*, but after three centuries the equilibrium value is reached again. The initial weakening of the THC results in a low-latitudinal oceanic temperature increase (Fig. 2,a) and a high-latitudinal oceanic temperature drop (Fig. 2,b) due to the reduced oceanic heat transport. Through surface heat fluxes low-latitudinal air temperatures rise (Fig. 3,a), while atmospheric temperatures in high latitudes decrease (Fig. 3,b). The resulting formation of snow and ice increases the albedo and leads to a further cooling. The resulting large meridional atmospheric temperature gradient causes higher eddy activity due to baroclinic instability. Consequently, atmospheric transports of heat (Fig. 4,b) and moisture (Fig. 4,a) intensify. The abrupt drop in low-latitudinal sea and air temperatures, occurring after a few years, is due to the increased poleward eddy heat transport. Variations in the total poleward heat transport (Fig. 4,d) are only small. The equilibrium total heat transport is determined by the radiation balance at the top of the atmosphere. Changes due to increased albedo are partly compensated by less outgoing longwave radiation. Therefore, anomalous oceanic heat transports are almost balanced

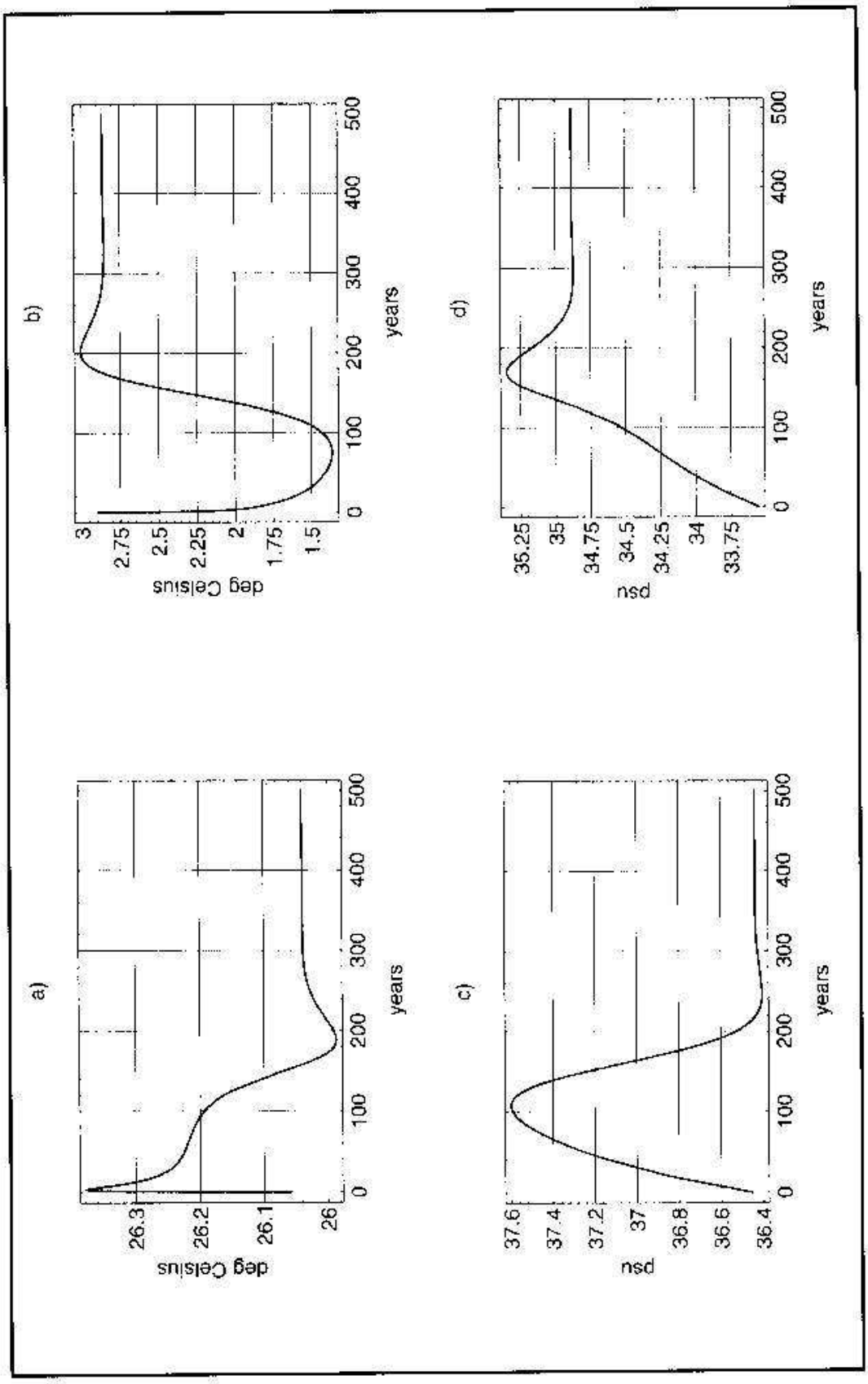

FIGURE 2 Time series of *a)* low-latitudinal sea surface temperature T_1, *b)* high-latitudinal sea surface temperature T_2, *c)* low-latitudinal sea surface salinity S_1, and *d)* high-latitudinal sea surface salinity S_2 after an initial salinity reduction in the high-latitudinal upper ocean box 2 slightly below the critical value $S_2' = 1.35$ *psu*. Due to the weakened thermohaline overturning sea temperatures initially rise in low latitudes and drop in the northern ocean. The THC recovers after about three centuries.

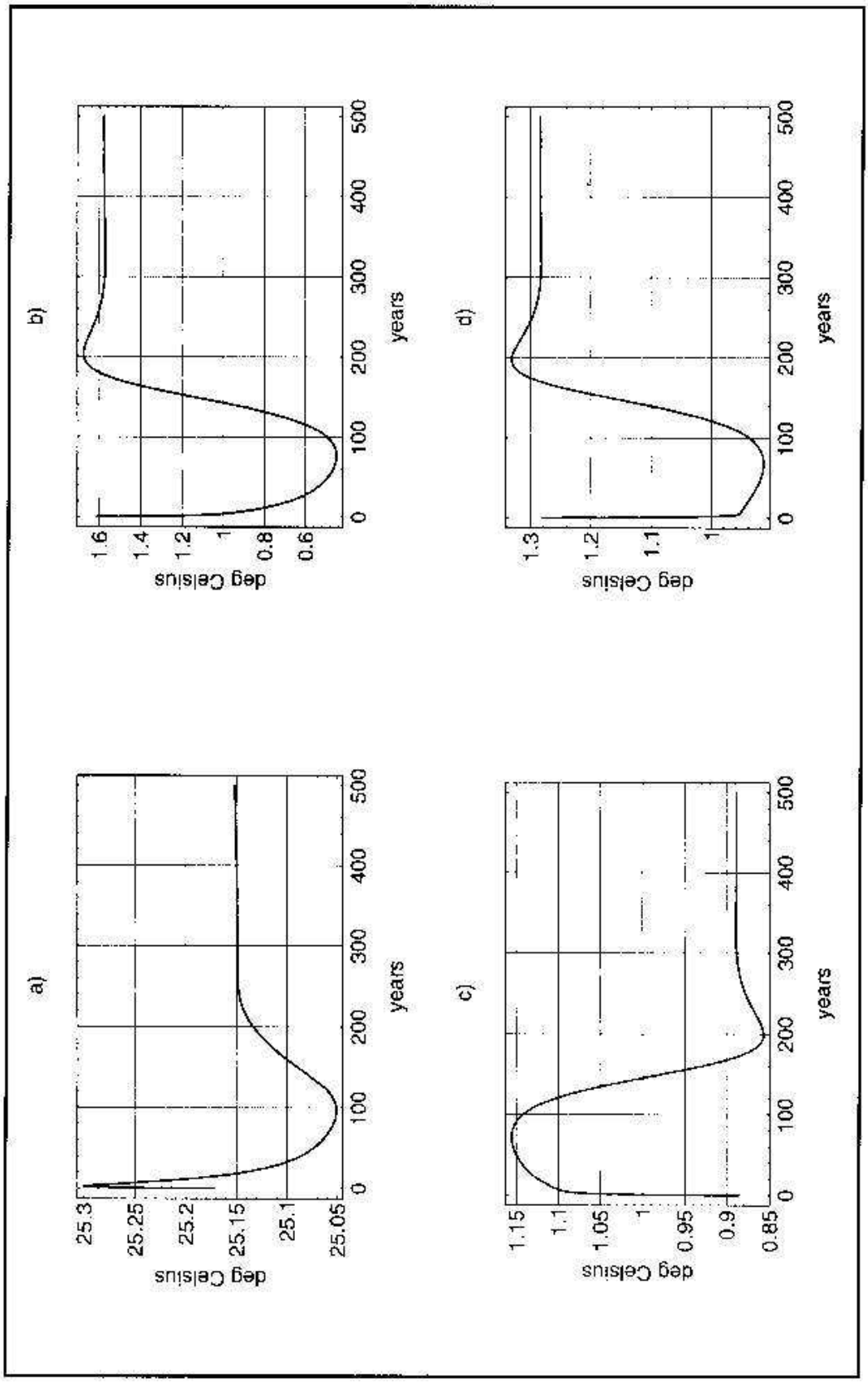

FIGURE 3 Time series of *a)* low-latitudinal surface air temperature $T_{a,1}$, *b)* high-latitudinal surface air temperature $T_{a,2}$, *c)* sea-air temperature difference in low latitudes, and *d)* sea-air temperature difference in high latitudes.

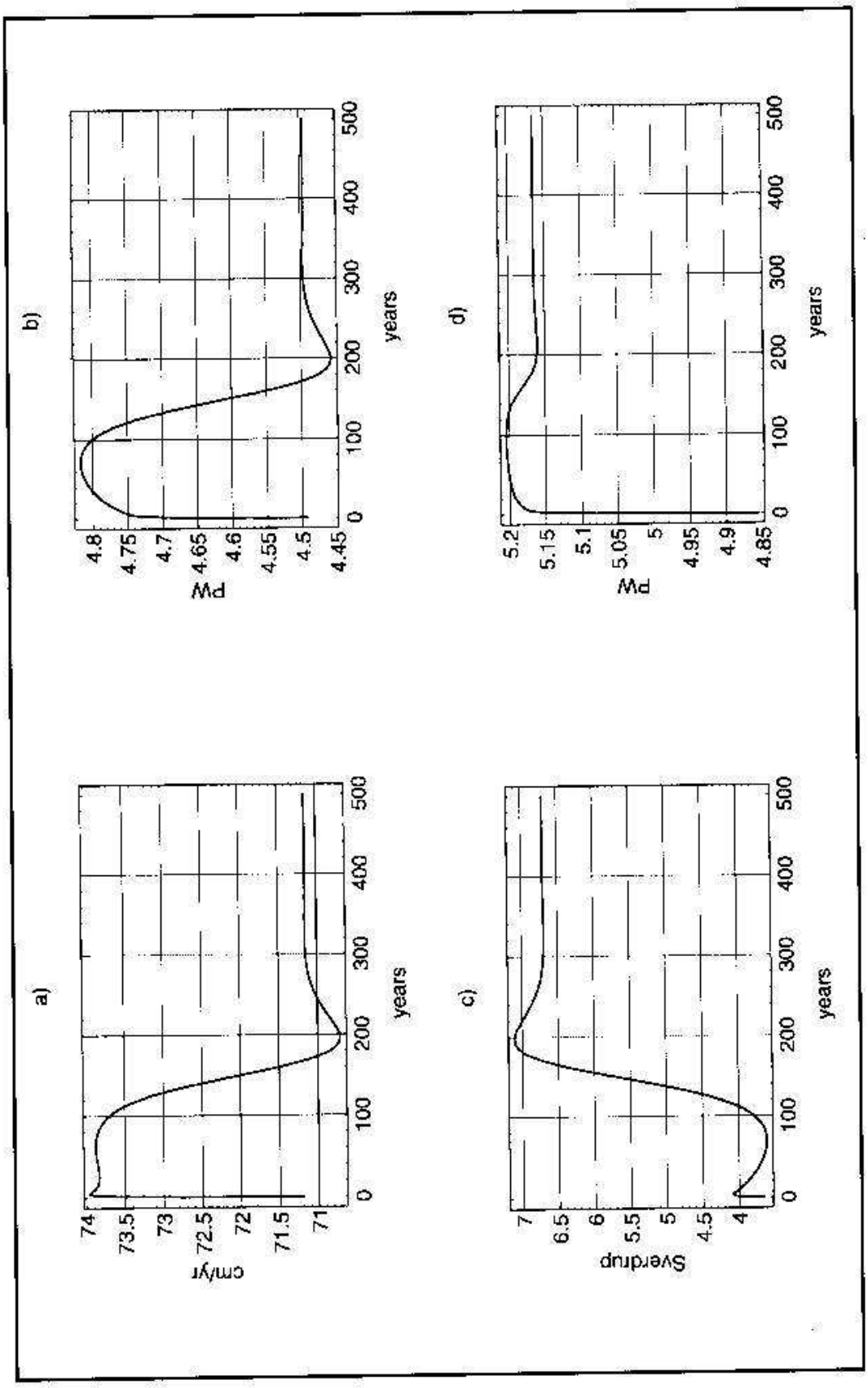

FIGURE 4 Time series of *a)* high-latitudinal freshwater forcing $A_1(P-E)_2$, *b)* poleward atmospheric heat transport $(F_s + F_l)$, *c)* thermohaline overturning rate q, and *d)* total northward heat transport of the ocean-atmosphere system. Atmospheric heat and freshwater fluxes initially raise due to increased eddy activity.

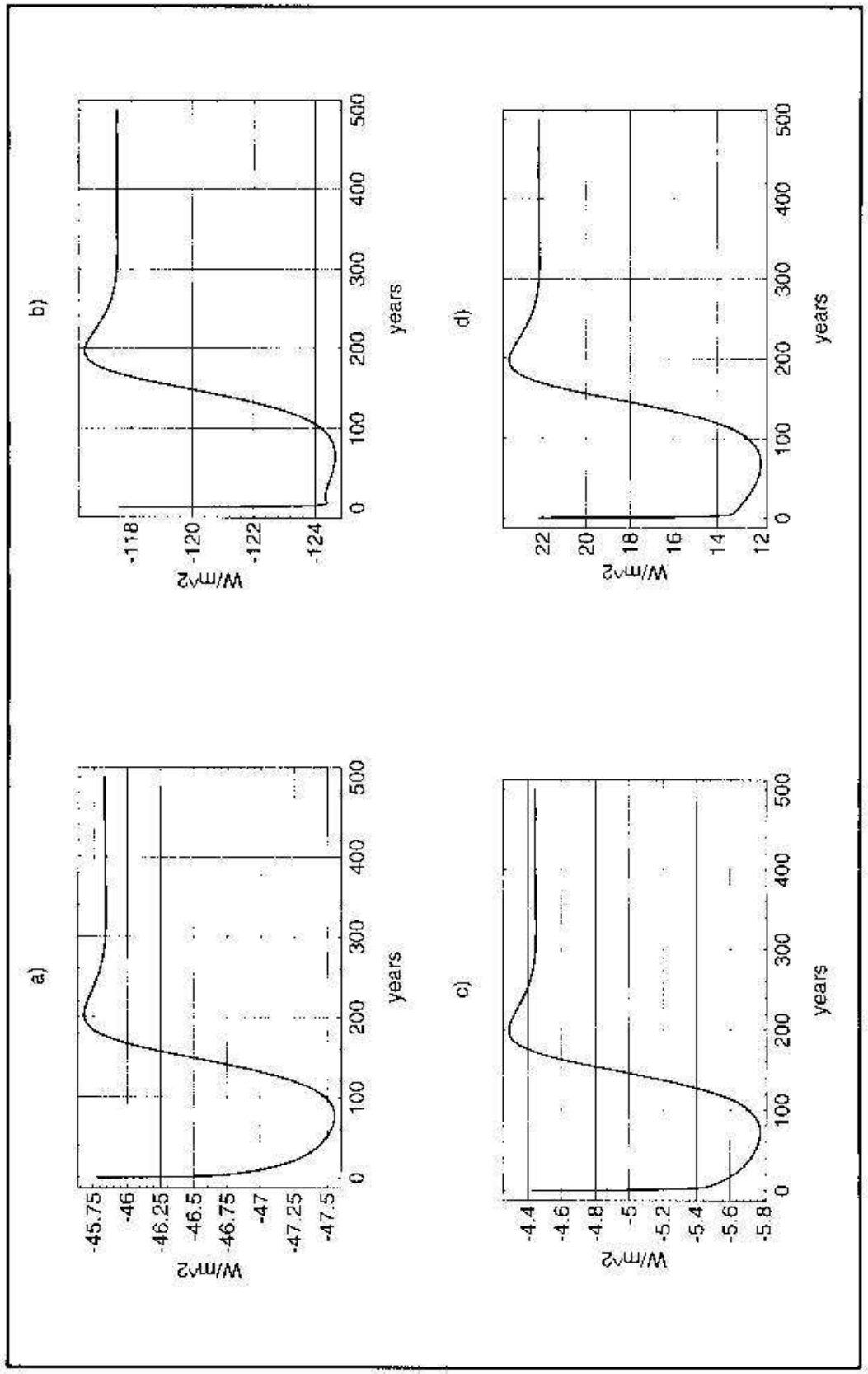

FIGURE 5 Time series of surface heat fluxes in low latitudes due to *a)* longwave radiation, *b)* latent heat exchange, and *c)* sensible heat exchange; *d)* shows the evolution of the total surface heat flux (negative signs indicate oceanic heat loss). Variations in surface heat fluxes cause sea surface temperature anomalies to remove, thus tending to destabilize the THC.

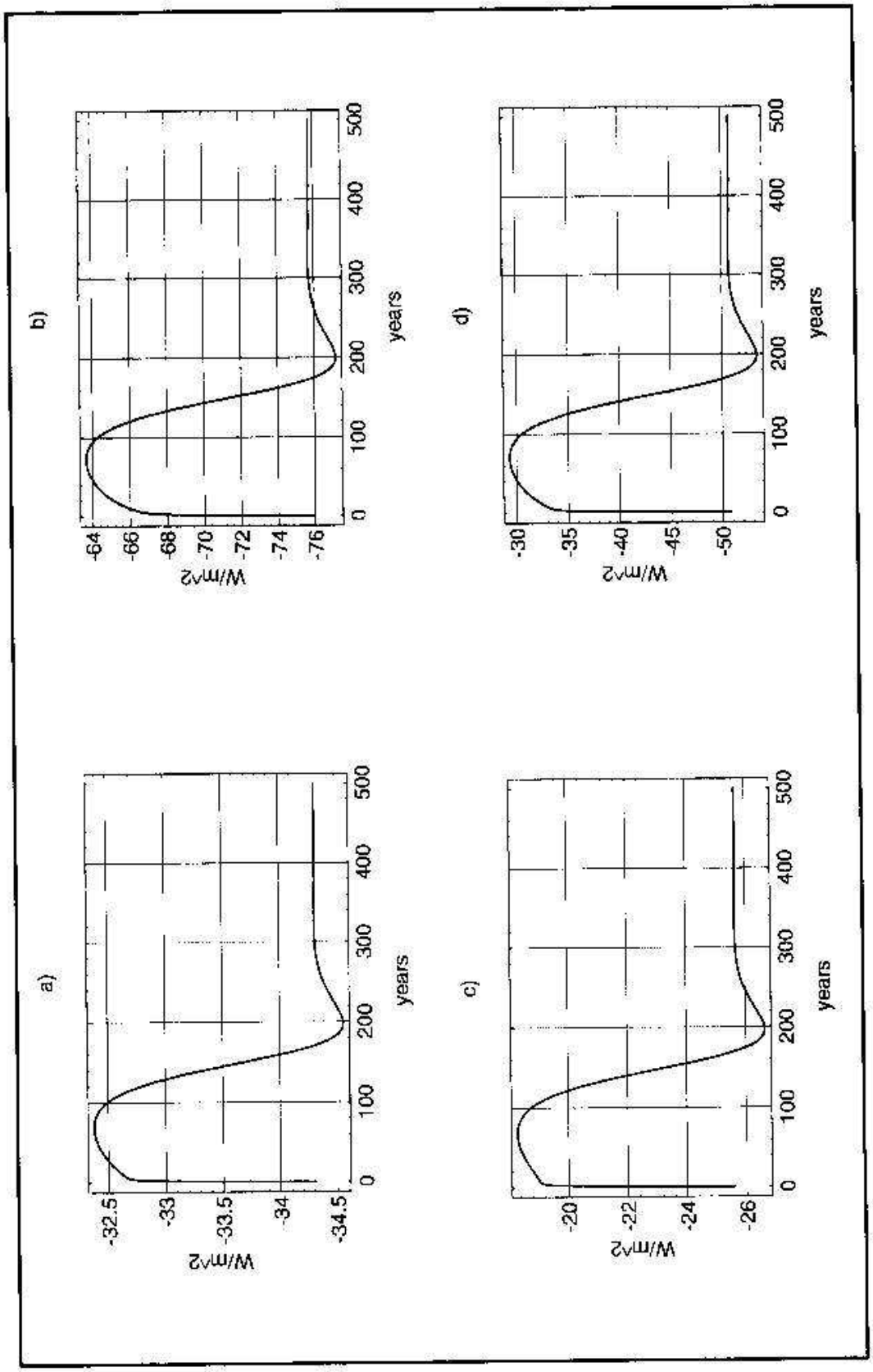

FIGURE 6 As Figure 5 but for high latitudes.

by anomalous atmospheric transports. The low-latitudinal salinity increase shown in Figure 2,c is caused by the intensified hydrologic cycle and by the reduced oceanic salt transport. The positive feedback between the northward oceanic salt transport and the meridional oceanic density gradient tends to destabilize the THC, whereas the negative feedback between the oceanic heat transport and the meridional density gradient has stabilizing impact. The former effect is reinforced by the negative feedback between oceanic overturning and atmospheric moisture transports, while the stabilizing latter effect is curtailed by variable surface heat fluxes (Figs. 5 and 6) which remove sea surface temperature anomalies. Variations in surface heat fluxes are mainly due to changed sea-air temperature differences. Figures 3,c and 3,d reveal that temperature variations in the ocean are actually larger than in the atmosphere, since air temperature anomalies are effectively removed by eddy transports and by longwave radiation to space according to (13). Thus, atmospheric heat advection as well as the longwave relaxation mechanism tend to destabilize the THC. Temperature and salinity of the deep-ocean box relax towards the high-latitudinal values with the large time constant V_3/q.

To demonstrate the importance of the atmospheric responses to large-scale oceanic circulation variations, stability experiments with simplified atmospheric model components are performed. The critical salinity reductions S_2' which cause a breakdown of the THC are listed in Table III for various models. In *model 2* the temperature-albedo feedback is excluded, and the THC turns out to be slightly more stable. The destabilizing impact of the temperature-albedo feedback can be attributed to a global cooling effect. The temperature-albedo feedback amplifies the high-latitudinal air temperature drop after an initial weakening of the THC. Due to atmospheric transports this additional cooling also affects low-latitude temperatures. Accordingly, low-latitudinal ocean temperatures do not rise as strong as they do with fixed planetary albedoes. Therefore, the temperature-albedo feedback tends to lower oceanic temperatures globally when the thermohaline overturning is disturbed. Since the thermal expansion coefficient of sea water $-\partial\rho_{o,i}/\partial T_i$ decreases linearly with temperature according to (8), the negative feedback between the oceanic heat transport and the meridional density gradient weakens in that case. In other words: Although an included temperature-albedo feedback enhances the meridional temperature gradient after an initial perturbation of the THC, it lessens the meridional density gradient of sea water. The effectiveness of atmospheric freshwater transports in *model 2* does not differ significantly from *model 1*. Freshwater transports depend on both the meridional temperature gradient and the absolute temperature according to (15). The effects of increased temperature gradients and decreased absolute temperatures in connection with a temperature-albedo feedback nearly cancel each other. This is confirmed by comparing the critical perturbations of *model 3* and *model 4* where

FIGURE 6 As Figure 5 but for high latitudes.

Table III Survey of the Investigated Models

Model	*Features*	S'_2 *[psu]*
1	– variable surface freshwater fluxes – variable planetary albedoes	1.35
2	– variable surface freshwater fluxes – planetary albedoes *fixed*	1.42
3	– surface freshwater fluxes *fixed* – planetary albedoes *fixed*	1.60
4	– surface freshwater fluxes *fixed* – variable planetary albedoes	1.54
5	– surface freshwater fluxes *fixed* – planetary albedoes *fixed* – simplified surface heat flux formulation with $Q_{1,i}$ and $Q_{2,i}$ *fixed*	1.64
6	– surface freshwater fluxes *fixed* – surface air temperatures *fixed* (i.e. *mixed boundary conditions*)	1.33
7	– surface freshwater fluxes *fixed* – planetary albedoes *fixed* – meridional atmospheric heat transports *fixed*	2.28
8	– surface freshwater fluxes *fixed* – sea-air temperature differences *fixed*	3.01
9	– surface freshwater fluxes *fixed* – surface heat fluxes *fixed*	—

The critical salinity reductions S'_2 are a measure for the stability of the THC with respect to freshwater perturbations in high latitudes. Exceeding the critical value S'_2 causes the current mode of the THC to collapse.

freshwater fluxes are fixed. The temperature-albedo feedback included in *model 4* has a destabilizing impact on the THC by the mechanisms explained above. The corresponding decrease in the critical salinity reduction S'_2 has about the same magnitude as in case of variable freshwater fluxes (*model 1* and *2*).

Apparently, the destabilizing effect of an included temperature-albedo feedback strongly depends on the efficiency of atmospheric heat transports (Fig. 8). If the power n in (14) and (15) is reduced, the cooling effect of the temperature-albedo feedback is restricted to high latitudes, and low-latitudinal oceanic temperatures can increase more strongly in consequence of a weakened oceanic circulation. In that case, the additional cooling effect in high latitudes acts to stabilize the thermohaline overturning. Additionally, the amplified high-latitudinal temperature drop results in a reduced atmospheric moisture transport and consequently in a more stable THC, when n is sufficiently small that the effect of decreased air temperature overcomes the effect of an increased meridional air temperature gradient in (15).

In order to study the influence of different surface heat flux parameterizations on the sensitivity of the model THC, both albedoes and surface freshwater fluxes

FIGURE 8 As Figure 5 but for high latitudes.

are fixed in the remaining models. *Model 5* differs from *model 3* by the heat flux coupling between the oceanic box model and the atmospheric EBM. Surface heat fluxes are now parameterized by

$$F_{oa,i} = Q_{1,i} - Q_{2,i}(T_i - T_{a,i}), \tag{25}$$

with $Q_{1,i}$ and $Q_{2,i}$ being constants. Such a parameterization is employed for instance in the coupled box models of Lohmann *et al.* (1996b) and Tang and Weaver (1995). To reproduce the equilibrium states of the previous models the following constants are required: $Q_{1,1} = 57.6\ W\,m^{-2}$, $Q_{2,1} = 40.0\ W\,m^{-2}{}^{\circ}C^{-1}$; $Q_{1,2} = 4.5\ W\,m^{-2}$, $Q_{2,2} = 43.2\ W\,m^{-2}{}^{\circ}C^{-1}$. *Model 5* yields a THC slightly more stable than *model 3*. This is mainly due to the inaccurate formulation of the oceanic latent heat losses to the atmosphere, which actually depend not only on sea-air temperature differences but also on absolute surface air temperatures according to (22). However, overestimated latent heat fluxes are partially compensated by underestimated sensible heat fluxes, so that the sensitivities of *model 3* and *model 5* differ only slightly. Thus, the linearized heat flux formulation (25) appears to be adequate.

In *model 6* air temperatures are kept fixed, so the frequently used mixed boundary conditions are reproduced. Mixed boundary conditions rule out any responses of the atmosphere to oceanic temperature variations and remove sea surface temperature anomalies very effectively. In oceanic GCMs typical restoring time scales of only a few weeks are linked up with mixed boundary conditions, resulting in extremely vulnerable oceanic circulations (*e.g.*, Zhang *et al.*, 1993; Lohmann *et al.*, 1996a; Cai and Godfrey, 1995; Rahmstorf and Willebrand, 1995). Although *model 6* is clearly more sensitive than *model 3*, the high sensitivities of GCMs can not be reproduced by the box model (see also Nakamura *et al.*, 1994). This can be attributed to the large upper ocean box depths Δz which determine the restoring time scales of sea surface temperature anomalies. Meridional atmospheric heat transports are fixed in *model 7*. Therefore, air temperature anomalies can only be removed by longwave radiation to space. Such an assumption is similar to the surface heat flux parameterization scheme proposed by Schopf (1983). Typical damping time scales for sea surface temperature anomalies are now about twenty times higher than with mixed boundary conditions, and the stability of the THC is strongly overestimated. The heat flux formulation suggested by Cai and Godfrey (1995) is employed in *model 8*. Here, sea-air temperature differences are fixed and sea surface temperature anomalies are mainly removed by latent heat fluxes which depend on surface air temperatures. Since this damping mechanism is only weak, temperature anomalies can persist on a long time scale, and the THC is extremely stabilized. Finally, in *model 9* both surface freshwater and heat fluxes are prescribed. A lasting destabilization

FIGURE 9 As Figure 5 but for high resolution.

of the THC is impossible now, since the equilibrium meridional transports are completely determined by the thermohaline forcing through surface fluxes.

Discussion

The response of the atmospheric model component to oceanic circulation variations strongly determines the sensitivity of the THC. If sea surface temperature anomalies are quickly removed through variable surface heat fluxes, the THC becomes more vulnerable. On the other hand, underestimating the variability of surface heat fluxes results in a strongly stabilized thermohaline overturning. In the present atmospheric EBM the atmospheric responses to a disturbed THC depend on the parameters β and n. β determines the heat capacity of the atmosphere. In Figure 7 the dependence of the critical salinity reduction S_2' on β is shown using *model 3*. The curve reveals that an exact determination of this parameter is rather unimportant, since the atmospheric heat capacity in the coupled system is actually negligible (the ocean's heat capacity is three orders of magnitude larger). However, if β is overestimated by a factor 100 or more, the critical perturbation S_2' decreases significantly. If β exceeds a value of 10^8 $kg\ m^{-2}$, air temperatures remain almost constant, and the critical perturbation approaches $S_2' = 1.33$ *psu* as in *model 6*. Thus, the limit of infinite atmospheric heat capacity corresponds to mixed boundary conditions.

The power n in (14) and (15) determines variations in atmospheric eddy activity as a result of large-scale temperature anomalies. By an empirical study, Stone and Miller (1980) found n to vary roughly from 1.6 at high latitudes to 4 at low

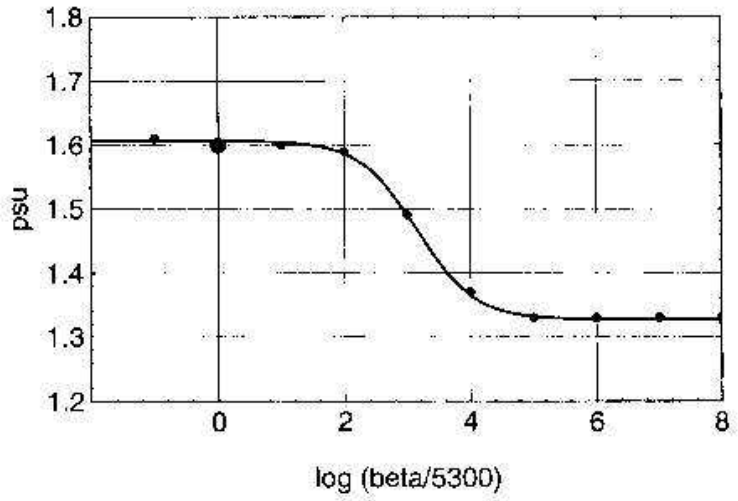

FIGURE 7 Dependence of the critical perturbation S_2' on β in *model 3*. The parameter β determines the heat capacity of the atmospheric model component. For sufficiently large β air temperatures remain almost constant, and the model corresponds to mixed boundary conditions.

latitudes. In model studies numerous different values are used. Nakamura *et al.* (1994) employ a power law with n being about 3.5, Lohmann *et al.* (1996a) use $n = 2$, Tang and Weaver (1995) $n = 4$. Several models employ a linear approach, *i.e.*, $n = 1$ (i.e., Chen *et al.*, 1995; Rahmstorf and Willebrand, 1995; Pierce *et al.*, 1996). Lohmann *et al.* (1996b) analyse their coupled box model by means of linear stability theory and show that linear instability of the THC is more likely to occur when high powers are employed. Perturbation experiments using *model 3* and various power laws yield critical salinities which are shown in Figure 8 (dashed line). For the limit of infinite n the model corresponds to mixed boundary conditions, since no air temperature anomalies can arise due to the instant removal by atmospheric heat transports. In that case S_2' approaches 1.33 *psu*. Thus, the use of mixed boundary conditions implies that any surface air temperature anomalies are instantly removed by atmospheric heat advection.

The solid line in Figure 8 shows critical salinity reductions for various n using *model 1* (variable atmospheric moisture transports and albedoes), while the dotted line shows the critical perturbations of *model 2* (albedoes fixed). For sufficiently large n the temperature-albedo feedback and the effect of variable freshwater fluxes act destabilizing. The effectiveness of atmospheric moisture transports in destabilizing the THC diminishes with decreasing power n. Additionally, the temperature-albedo feedback tends to stabilize the THC for small n (see previous section). Consequently, *model 1* turns out to be even more stable than *model 3* when n approaches zero. In case of very large n ($n > 50$) *model 1* is slightly more stable than *model 2* due to a short-term global cooling and reduced atmospheric freshwater fluxes in consequence of the temperature-albedo feedback.

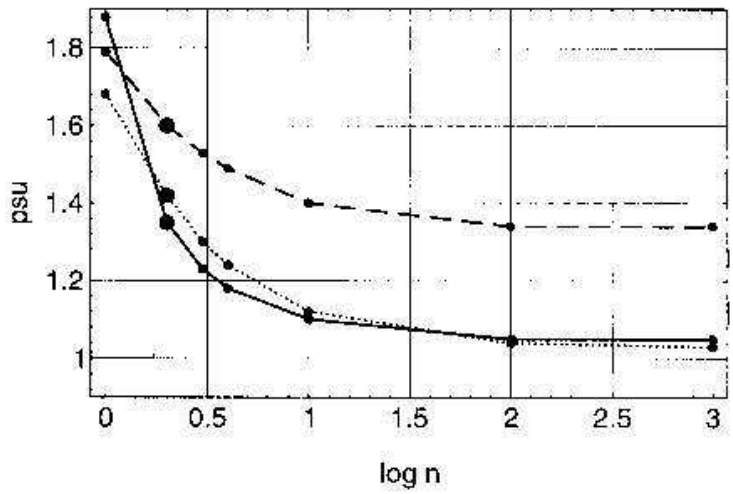

FIGURE 8 Dependence of the critical perturbation S_2' on n in *model 1* (solid line), *model 2* (dotted line), and *model 3* (dashed line). n determines the strength of eddy activity variations due to a weakened THC. The large dots correspond to $n = 2$. For sufficiently low n the temperature-albedo feedback in *model 1* acts strongly stabilizing.

The destabilizing effect of eddy moisture transports is already pointed out in the box model study of Nakamura *et al.* (1994). However, it appears that their coupled model strongly overestimates the efficiency of this mechanism, since it calculates atmospheric transports at relatively low latitudes (35°*N*). As low-latitudinal temperatures tend to increase significantly in consequence of a weakened THC, Nakamura *et al.* (1994) overrate the effect of the hydrologic cycle. By way of contrast, the coupled oceanic GCM-atmospheric EBM experiments of Lohmann *et al.* (1996a) exhibit an almost negligible influence of the hydrologic cycle on the sensitivity of the THC. However, their model ignores continental runoff and hence underestimates the freshwater input into the northern North Atlantic. Rahmstorf and Willebrand (1995) as well as Pierce *et al.* (1996) also couple an oceanic GCM with an atmospheric EBM. They use a linear power law (*i.e.*, $n = 1$) for atmospheric heat transports and prescribe surface freshwater fluxes. Thus, the stability of the THC in these models is probably overestimated. Sensitivity studies with coupled atmospheric and oceanic GCMs (Manabe and Stouffer, 1995) must also be interpreted with caution, since these models need large adjustments of surface heat and freshwater fluxes to maintain a realistic thermohaline overturning (Sausen *et al.*, 1988; Manabe and Stouffer, 1988). Such adjustments can considerably affect the sensitivity of the THC (*e.g.*, Lohmann, 1995).

3. THE SENSITIVITY OF THE THC IN DIFFERENT CLIMATES

Producing Different Climatic States

Stability investigations with the present box model are performed to get some insights into the sensitivity of the THC in warmer and colder climates than the current one. The global climate can be altered by changing the radiation balance at the top of the atmosphere. Following Budyko (1977) the effect of atmospheric greenhouse gases can be simulated by varying the parameterization for the longwave emission I_i in (13). This can be realized by multiplying I_i by a factor γ which depends on greenhouse gas concentration only.

The simple box model can not reliably describe large deviations from the current climate, because the tuning is based on present-day climatology, and important physical processes might not be included. Especially the lack of an interactive sea ice component limits the scope of the present box model, as large changes of sea ice patterns can have a strong impact on surface heat fluxes and hence on the entire dynamics of the THC (*e.g.*, Lohmann and Gerdes, 1996). Therefore, γ should not differ too much from 1.0 in a box model. Considering this limitation, γ is chosen to be 1.002 for the simulation of a colder climate. A warmer climate is

obtained by setting $\gamma = 0.998$. This procedure provides reasonable climate states whose main characteristics are listed in Table II. Due to the lack of the Pacific's large heat storage the model appears to be rather sensitive to radiative forcing. The colder climate is associated with a global atmospheric cooling of 2.02°C, while the warming scenario corresponds to a global air temperature increase of 1.56°C. Changes in net radiation at the top of the atmosphere amount to $\Delta R_t = +0.73 W m^{-2}$, $\Delta R_t = -1.70 W m^{-2}$ for the global cooling scenario, and $\Delta R_t = -0.63 W m^{-2}$, $\Delta R_t = +1.52 W m^{-2}$ for the warmer climate. Note that high-latitudinal and low-latitudinal radiation changes have opposite signs, since net radiation in low latitudes is mainly affected by changes in thermal longwave emission, whereas this effect is more than compensated by altered albedoes in high latitudes. In equilibrium these changes in radiative fluxes must be compensated for through meridional fluxes in the atmosphere-ocean system. Accordingly, the total poleward heat transport increases in the colder climate and decreases in consequence of a global warming. The increase in heat transport in the cold epoch is accomplished by an augmentation in atmospheric sensible heat transports due to the enhanced meridional air temperature gradient ($\Delta(T_{a,1} - T_{a,2}) = +1.27°C$). Atmospheric latent heat (and hence freshwater) transports diminish owing to the decreased moisture capacity of the cooled air. By way of contrast, a global warming is accompanied by meridional air temperature gradient decrease ($\Delta(T_{a,1} - T_{a,2}) = -0.93°C$), sensible heat transport reduction, and poleward latent heat flux augmentation.

The weakening of the thermohaline overturning in the colder climate despite the enhanced meridional temperature gradient ($\Delta(T_1 - T_2) = +1.46°C$) can be attributed to the temperature-dependence of the thermal expansion coefficient of sea water. The increase in density in low latitudes amounts of $\Delta\rho_{o,}1 = +0.72\ kg\ m^{-3}$ according to (8), and predominates over the density increase in high-latitudinal waters ($\Delta\rho_{o,}2 = +0.12 kg\ m^{-3}$), since the thermal expansion coefficient $-\partial\rho_{o,i}/\partial T_i$ is lower in high (cold) than in low (warm) latitudes. Accordingly, the THC strengthens when a global warming takes place, although the meridional temperature gradient decreases ($\Delta(T_1 - T_2) = -0.95°C$). The positive feedback between northward salt transport and thermohaline overturning amplifies the THC's tendency to weaken or to strengthen, although altered atmospheric moisture transports tend to counteract this effect. However, it appears that the corresponding surface freshwater flux changes are only of minor importance compared to the changes in oceanic salt transports. Table II reveals that the salinity contrast $S_1 - S_2$ actually increases in the global cooling scenario, whereas it is reduced in the warmer climate. If atmospheric freshwater transports were assumed to remain at the present-day value, the THC would increase to 7.78 *Sv* with respect to global warming instead of 7.60 *Sv* (Table II) when moisture transports are allowed to rise.

Comparison with Other Studies

During the last glacial maximum (LGM), 18,000 years B.P. (radiocarbon date), which corresponds to the last maximum extent of the Laurentide and Fennoscandian ice sheets, the global annual mean surface air temperature is supposed to be approximately $4°C$ less than today (*e.g.*, COHMAP, 1988; Joussaume, 1993). On the other hand, doubled CO_2 studies with atmospheric GCMs predict global warmings of up to $4.8°C$ (Watterson and Dix, 1996). The new box model climates (Table II) have several *qualitative* agreements with LGM and doubled CO_2 scenarios discussed in the following:

- Temperature changes due to radiative forcing are larger in high than in low latitudes in consequence of polar amplification by the temperature-albedo feedback. Hence, mean meridional temperature gradients increase when a global cooling takes place. Atmospheric GCMs in conjunction with CLIMAP (1981) surface boundary conditions show a cooling of roughly $11°C$ above $60°N$, and of only $1.2°C$ in tropical regions (*e.g.*, Joussaume, 1993) for the LGM. However, recent geochemical studies provide some support for the hypothesis that tropical sea surface temperatures may have been $2°–3°C$ colder than estimated by CLIMAP (Guilderson *et al.*, 1994). GCM CO_2 doubling studies show a mean warming of roughly $5°–7°C$ above $60°N$, and lower temperature changes near the equator of only about $2°–3°C$ (*e.g.*, Meehl and Washington, 1990), so that the mean meridional surface air temperature gradient decreases.
- The enhanced mean meridional air temperature gradient during the LGM is connected with increased baroclinicity, and hence with a larger poleward *energy flux in the atmosphere*. Hall *et al.* (1996) find an increase of about 1 *PW* in the northern hemisphere at the LGM in the annual mean.
- The signs of changes in *net radiation balance at the top of the atmosphere* at the LGM in the annual mean are consistent with those obtained in the box model's colder climate (Hall *et al* 1996). Accordingly, the total northward heat transport by the ocean and the atmosphere becomes larger in colder climates.
- Numerous CO_2 doubling simulations show an intensified *atmospheric freshwater transport* owing to the increased moisture capacity of the warmed air (*e.g.*, Manabe and Bryan, 1985; Manabe and Stouffer, 1993; Hall *et al.*, 1994), whereas LGM studies reveal a weakened hydrologic cycle (*e.g.*, Joussaume, 1993).
- By means of a coupled atmosphere-ocean GCM with idealized one hemisphere geometry Manabe and Bryan (1985) find an intensification of the *meridional oceanic circulation* with increasing global temperature due to the temperature-dependence of the thermal expansion coefficient of sea water. GCMs driven with LGM boundary conditions exhibit that the THC in the Atlantic ocean

was considerably weaker under glacial conditions than today, while the Pacific circulation was almost identical to its present-day pattern (*e.g.*, Hovine and Fichefet, 1994; Winguth *et al.*, 1996). These findings are confirmed by geological reconstructions (*e.g.*, Boyle and Keigwin, 1987; Curry *et al.*, 1988; Duplessy *et al.*, 1988).

- Reconstructions by Duplessy *et al.* (1991) show that the *sea surface salinity* contrast between low and high latitudes was larger during the LGM than today. Since only the meridional salinity gradient enters (7), the absolute global salinity is unimportant in the box model.
- The *mean planetary albedo* is larger in the colder climate than under present-day conditions. The LGM study of Joussaume (1993) provides a planetary albedo increase of 2.45% for the northern hemisphere in the annual mean.
- Watterson and Dix (1996) analyze *surface energy fluxes* simulated by an atmospheric GCM for present-day and doubled CO_2 conditions. In consequence of the warming, they find a global decrease in oceanic heat losses through longwave emission and strongly enhanced latent heat losses. The former effect is attributed to a global increase in downward longwave radiation from the atmosphere to the ocean, while the latter effect is connected with the enhanced saturation specific humidity and hence intensified evaporation. In high latitudes the latent heat fluxes increase by roughly about 15 $W\,m^{-2}$. In the same way, latent heat losses globally increase in the present box model study in consequence of a global warming. In high latitudes intensification of latent heat fluxes is particularly strong and is the main reason for the enhanced net heat loss. In low latitudes the weak increase in latent heat fluxes is more than compensated by a decrease in net longwave emission. For the global cooling scenario the net heat loss decreases in high latitudes, which can mainly be attributed to lessened latent heat fluxes. In low latitudes the net heat gain of the ocean decreases due to increased longwave radiation losses.

To sum it up it can be said that the coupled box model captures some features which are associated with global temperature changes. This is an important basis for the validity of the following stability investigations.

Stability Investigations

Stability investigations concerning the new equilibrium states give critical salinity perturbations of $S_2' = 0.40$ *psu* and $S_2' = 1.86$ *psu* for the colder and the warmer climate, respectively. Comparing these values with the critical salinity perturbation of the current climate $S_2' = 1.35$ *psu* reveals that the THC is stabilized

by the global warming, whereas it becomes considerably more vulnerable in the cooler climate.

These results are compatible with those of Lohmann *et al.* (1996b) insofar as a strong equilibrium overturning is linked up with high stability. When the equilibrium circulation weakens it becomes more vulnerable. Lohmann *et al.* (1996b) deal with the linear stability of a coupled box model with regard to different equilibrium states. In their model a weakening of the equilibrium THC can be realized either by increasing the meridional salinity contrast or by decreasing the meridional temperature gradient. Since the model of Lohmann *et al.* (1996b) assumes a linear dependence of sea water density on temperature (*i.e.*, the thermal expansion coefficient is a constant), absolute oceanic temperatures play no role, and the thermohaline overturning strength as well as its stability is determined by meridional gradients only. By way of contrast, the present study reveals the importance of the temperature-dependence of the thermal expansion coefficient. The THC weakens and becomes more vulnerable with respect to global cooling despite an enhanced meridional oceanic temperature gradient. Additionally, a second effect arises due to the temperature-dependence of the thermal expansion coefficient in the present study: The stabilizing negative feedback between the oceanic heat transport and the meridional sea water density gradient lessens when thermal expansion coefficients diminish due to global cooling. In warmer climates this feedback strengthens owing to the elevation of the thermal expansion coefficient, and the THC is additionally stabilized.

In order to estimate the importance of both non-linear effects, the three equilibrium states of Table II (present-day, colder and warmer climate) are perturbed using a linear equation of state, *i.e.*, high- and low-latitudinal thermal expansion coefficients of the present-day climate are calculated and fixed throughout. The factor c in (7) is adjusted properly to reproduce the equilibrium overturning rates q of the colder and the warmer climate. The stability experiments give critical salinity perturbations of $S_2' = 0.48$ *psu*, 1.21 *psu* and 1.54 *psu* for the colder, the current and the warmer climate, respectively. The results indicate that the first effect (*i.e.*, high stability due to a strong equilibrium overturning) may be the more important one, but that the second non-linear effect (strengthened feedback between heat transport and meridional density gradient due to increased thermal expansion coefficients) is still not negligible for climate variability.

Palaeoclimatic Interpretation

Meltwater invasions into the North Atlantic owing to retreating glaciers are assumed to be responsible for abrupt climate changes like the Younger Dryas cold event 11,000 years B.P. (Broecker, 1991). Sediment layers in the North Atlantic

ocean (Heinrich layers), deposited between 14,000 and 70,000 years ago, record considerable decreases in sea surface temperature and salinity, and massive discharges of icebergs originating in eastern Canada (Bond *et al.*, 1992), leading to the conclusion that armadas of icebergs also might have caused sudden climatic fluctuations. The present results indicate that during glacial epochs the THC was much more susceptible to such freshwater perturbations than today. Thus, even relatively small perturbations might have caused considerable variations in the intensity of the THC accompanied by severe cold snaps in high latitudes due to the weakened oceanic heat transport.

GCM studies of Rahmstorf (1994) and Lohmann and Gerdes (1996) show that freshwater perturbations may cause a transition of the THC into different climate states with shallower convection where the sites of deep water formation areas shift southward. The resulting circulation pattern is associated with lower surface heat fluxes in northern regions and hence a lasting cooling in high latitudes. There is palaeoclimatic evidence which indicates strengthened intermediate ocean currents and weakened deep water flows during the Younger Dryas (McCave *et al.*, 1995), thus confirming the model findings. Such a transition of the THC might explain the long duration of the Younger Dryas cold period (about 1,300 years).

The present-day oceanic circulation is substantially more stable with respect to freshwater perturbations than the circulation of past glacial epochs. The high stability of today's THC could be *one* reason for the equable climate during the last 10,000 years. By way of contrast, the high sensitivity of the oceanic circulation in Ice Ages leads to high climate variability.

4. CONCLUSIONS

An oceanic box model was coupled with an atmospheric EBM. The sensitivity of the THC was studied with regard to different surface flux parameterization schemes and climates. The model reveals the importance of atmospheric responses to oceanic circulation variations. Both atmospheric heat and moisture transports tend to destabilize the THC. Thus, neglecting these transports in model calculations, as proposed by Schopf (1983), results in an artificial overstabilization. On the other hand, if atmospheric heat transports are overestimated, the stability of the THC is considerably reduced. This happens when mixed boundary conditions are employed. Apparently, neither Schopf's approach nor mixed boundary conditions are appropriate to sensitivity or variability studies. An atmospheric EBM is a suitable tool for estimating atmospheric responses. A simplified coupling between the oceanic and the atmospheric model component by means of a linearized heat flux parameterization turns out to be adequate.

The box model is not able to determine clearly whether a temperature-albedo feed-back stabilizes or destabilizes the thermohaline overturning. It is a certainty that a temperature-albedo feedback reinforces the high-latitudinal temperature drop after an initial perturbation of the oceanic circulation. The additional cooling tends to stabilize the THC. However, if the efficiency of atmospheric heat transports is large enough, this cooling is transmitted to low latitudes, and a global cooling tendency occurs. Since the thermal expansion coefficient of sea water decreases with temperature, the negative feedback between the oceanic heat transport and the meridional density gradient weakens. Consequently, a temperature-albedo feedback tends to destabilize the THC if atmospheric heat transports are very powerful, otherwise a temperature-albedo feedback stabilizes the circulation.

The stability investigations in different climates have particular palaeoclimatic importance. In that case, the dependence of the thermal expansion coefficient on temperature turns out to be of paramount importance. It causes the THC to strengthen in a warmer climate and to weaken in a cold epoch. Furthermore, increased thermal expansion coefficients enhance the stability of the THC in warmer climates, whereas the stability lessens in Ice Ages. Thus, the THC was probably more vulnerable in past glacial epochs than today. Even relatively small freshwater infusions owing to melting glaciers or icebergs might have caused considerable changes in the THC, leading to high variability of the climate system.

Convective processes, which are not considered in the box model, can have additional impact on the stability of the oceanic circulation. A convective instability mechanism is analysed for different climates by Winton (1997) using Schopf's boundary conditions. He shows that North Atlantic Deep Water formation is favored by a warm climate due to the non-linearity of the equation of state. In colder climates the convection is more susceptible to stratification by surface freshening.

For future studies more sophisticated coupled models with sufficiently high resolutions should run under different climatic conditions to deepen the insights obtained with the present model. Local processes can not be considered with a simple box model. In particular, sea ice effects may play an essential role, affecting the sensitivity of the THC. Recent models of Zhang *et al.* (1995), Lenderink and Haarsma (1996) and Lohmann and Gerdes (1996) include thermodynamic sea ice models to study today's THC. However, only Lohmann and Gerdes (1996) take account of atmospheric feedbacks due to eddy activity. They find an important impact of sea ice on the sensitivity of the THC owing to changed surface heat fluxes. Due to their ability to shift the sea ice margin poleward, atmospheric heat transports appear to have a stabilizing effect on the THC in that case.

Despite its simplicity the presented box model provides many insights into important feedback mechanisms which are connected with the THC. Much work

has still to be done to understand the THC's sensitivity under different climatic conditions and to grasp climate variability as a whole.

Acknowledgements

We thank Prof. Dr. D.J. Olbers and Prof. Dr. K. Hasselmann for their support. This paper is contribution number 1215 from Alfred-Wegener-Institute for Polar and Marine Research.

References

Bond, G.C., Heinrich, H., Broecker, W., Labeyrie, L., McManus, J., Andrews, J., Huon, S., Jantschik, R., Clasen, S., Simet, C., Tedesco, K., Klas, M., Bonani, G. and Ivy, S. (1992) Evidence for massive discharges of icebergs into the North Atlantic ocean during the last glacial period. *Nature*, **360**, 245–249.

Bond, G.C. (1995) Climate and the conveyor. *Nature*, **377**, 383–384.

Boyle, E.A. and Keigwin, L.D. (1987) North Atlantic thermohaline circulation during the last 20,000 years linked to high latitude surface temperature. *Nature*, **330**, 35–40.

Branscome, L.E. (1983) A parameterization of transient eddy heat flux on a beta plane. *Journal of Atmospheric Science*, **40**, 2508–2521.

Broecker, W.S. (1991) The great ocean conveyor. *Oceanography*, **4**, 79–89.

Bryan, F. (1986) High-latitude salinity effects and interhemispheric thermohaline circulations. *Nature*, **323**, 301–304.

Budyko, M.I. (1969) The effect of solar radiation variations on the climate of the earth. *Tellus*, **21**, 611–619.

Budyko, M.I. (1977) *Climatic Changes*. Washington, D.C.: American Geophysical Union.

Cai, W. and Godfrey, S.J. (1995) Surface heat flux parameterizations and the variability of thermohaline circulation. *Journal of Geophysical Research*, **100**, 10679–10692.

Chen, D., Gerdes, R. and Lohmann, G. (1995) A 1-D atmospheric energy balance model developed for ocean modelling. *Theoretical and Applied Climatology*, **51**, 25–38.

CLIMAP (Climate: Long range investigation, mapping and prediction) (1981) Seasonal reconstructions of the earth's surface at the Last Glacial Maximum. *Geological Society of America*, Map chart series MC-36, Boulder, Colorado.

COHMAP members (1988) Climatic changes of the last 18,000 years: Observations and model simulations. *Science*, **241**, 1043–1052.

Curry, W.B., Duplessy, J.-C., Labeyrie, L.D. and Shackleton, N.J. (1988) Changes in the distribution of $\delta^{13}C$ of deep water ΣCO_2 between the last glaciation and the Holocene. *Paleoceanography*, **3**, 317–341.

Duplessy, J.-C., Shackleton, N.J., Fairbanks, R.G., Labeyrie, L.D., Oppo, D. and Kallel, N. (1988) Deepwater source variations during the last climatic cycle and their impact on the global deepwater circulation. *Paleoceanography*, **3**, 343–360.

Duplessy, J.-C., Labeyrie, L.D., Juillet-Leclerc, A., Maitre, F., Duprat, J. and Sarnthein, M. (1991) Surface salinity reconstruction of the North Atlantic Ocean during the Last Glacial Maximum. *Oceanologica Acta*, **14**, 311–324.

Fanning, A.F. and Weaver, A.J. (1996) An atmospheric energy-moisture balance model: Climatology, interpentadal climate change, and coupling to an OGCM. *Journal of Geophysical Research*, submitted.

Griffel, D.H. and Drazin, P.G. (1981) On diffusive climatological models. *Journal of Atmospheric Science*, **38**, 2327–2332.

Guilderson, T.P., Fairbanks, R.G. and Rubenstone, J.L. (1994) Tropical temperature variations since 20,000 years ago: Modulating interhemispheric climate change. *Science*, **263**, 663–665.

Hall, N.M.J., Hoskins, B.J., Valdes, P.J. and Senior, C.A. (1994) Storm tracks in a high resolution GCM with doubled carbon dioxide. *Quarterly Journal of the Royal Meteorological Society*, **120**, 1209–1230.

Hall, N.M.J., Dong, B. and Valdes, P.J. (1996) Atmospheric equilibrium, instability and energy transport at the Last Glacial Maximum. *Climate Dynamics*, **12**, 497–511.

Haney, R.L. (1971) Surface thermal boundary condition for ocean circulation models. *Journal of Physical Oceanography*, **1**, 241–248.

Hasse, L. (1993) Observations of air sea fluxes. In *Energy and Water Cycles in the Climate System*, NATO ASI Series. E. Raschke and D. Jacob (eds.) pp. 263–293. Berlin, Heidelberg: Springer-Verlag.

Hovine, S. and T. Fichefet (1994) A model study of the glacial oceanic circulation. In *Long-Term Climatic Variations*, NATO ASI Series. J.-C. Duplessy and M.-T.Spyridakis (eds) pp. 481–489. Berlin, Heidelberg: Springer-Verlag.

Isemer, H.J. and Hasse, L. (1987) *The Bunker climate atlas of the North Atlantic Ocean. Vol 2: Air-sea interactions*. Berlin, Heidelberg, New York: Springer-Verlag.

Joussaume, S. (1993) Paleoclimatic tracers: An investigation using an atmospheric general circulation model under Ice Age conditions, part 1: Desert dust. *Journal of Geophysical Research*, **98**, 2767–2805.

Keigwin, L.D., Jones, G.A., Lehman, S.J. and Boyle, E.A. (1991) Deglacial melt-water discharge, North Atlantic deep circulation, and abrupt climate change. *Journal of Geophysical Research*, **96**, 16811–16826.

Lenderink, G. and Haarsma, R.J. (1996) Modeling convective transitions in the presence of sea-ice. *Journal of Physical Oceanography*, **26**, 1448–1467.

Lohmann, G. (1995) Stability of the thermohaline circulation in analytical and numerical models. Ph.D. thesis, University of Bremen. *Reports on Polar Research*, **200**, Alfred-Wegener-Institute for Polar and Marine Research, Bremerhaven.

Lohmann, G., Gerdes, R. and Chen, D. (1996a) Sensitivity of the thermohaline circulation in coupled oceanic GCM-atmospheric EBM experiments. *Climate Dynamics*, **12**, 403–416.

Lohmann, G., Gerdes, R. and Chen, D. (1996b) Stability of the thermohaline circulation in a simple coupled model. *Tellus*, **48a**, 465- 477.

Lohmann, G. and Gerdes, R. (1996) Sea ice effects on the sensitivity of the thermohaline circulation. *Journal of Climate*, in press.

Maas, L.R.M. (1994) A simple model for the three-dimensional thermally and wind-driven ocean circulation. *Tellus*, **46a**, 671–680.

Manabe, S. and Bryan, K. (1985) CO_2-induced change in a coupled ocean-atmosphere model and its paleoclimatic implications. *Journal of Geophysical Research*, **90**, 11689–11707.

Manabe, S. and Stouffer, R.J. (1988) Two stable equilibria of a coupled ocean-atmosphere model. *Journal of Climate*, **1**, 841–863.

Manabe, S. and Stouffer, R.J. (1993) Century-scale effects of increased atmospheric CO_2 on the ocean-atmosphere system. *Nature*, **364**, 215–218.

Manabe, S. and Stouffer, R.J. (1995) Simulation of abrupt climate change induced by freshwater input to the North Atlantic Ocean. *Nature*, **378**, 165–167.

McCave, N., Manighetti, B. and Beveridge, N.A.S. (1995) Circulation in the glacial North Atlantic inferred from grain-size measurements. *Nature*, **374**, 149–151.

Meehl, G.A. and Washington, W.M. (1990) CO_2 climate sensitivity and snow-sea-ice parameterization in an atmospheric GCM coupled to a mixed-layer ocean model. *Climatic Change*, **16**, 283–306.

Michaud, R. and Derome, J. (1991) On the mean meridional transport of energy in the atmosphere and oceans as derived from six years of ECMWF analyses. *Tellus*, **43a**, 1–14.

Nakamura, M., Stone, P.H. and Marotzke, J. (1994) Destabilization of the thermohaline circulation by atmospheric eddy transports. *Journal of Climate*, **7**, 1870–1882.

Oberhuber, J.M. (1988) An atlas based on the COADS data set: The budgets of heat, buoyancy and turbulence kinetic energy at the surface of the global ocean. Max-Planck-Institute for Meteorology, Hamburg, Report No. 15.

Oort, A.H. and Peixoto, J.P. (1983) Global angular momentum and energy balance requirements from observations. *Advances in Geophysics*, **25**, 355–490.

Pierce, D.W., Kim, K.-Y. and Barnett, K.P. (1996) Variability of the thermohaline circulation in an ocean general circulation model coupled to an atmospheric energy balance model. *Journal of Physical Oceanography*, **26**, 725–738.

Rahmstorf, S. (1994) Rapid climate transitions in a coupled ocean-atmosphere model. *Nature*, **372**, 82–85.

Rahmstorf, S. and Willebrand, J. (1995) The role of temperature feedback in stabilizing the thermohaline circulation. *Journal of Physical Oceanography*, **25**, 787–805.

Sausen, R., Barthels, R.K. and Hasselmann, K. (1988) Coupled ocean-atmosphere models with flux correction. *Climate Dynamics*, **2**, 154–163.

Schopf, P.S. (1983) On equatorial waves and El Nino. II: Effects of air-sea thermal coupling. *Journal of Physical Oceanography*, **13**, 1878–1893.

Shuttleworth, W.J. (1993) The soil-vegetation-atmosphere interface. In *Energy and Water Cycles in the Climate System*, NATO ASI Series. E. Raschke and D. Jacob (eds) pp. 323–364. Berlin, Heidelberg: Springer-Verlag.

Stocker, T.F., Wright, D.G. and Mysak, L.A. (1992) A zonally averaged, coupled ocean-atmosphere model for paleoclimate studies. *Journal of Climate*, **5**, 773–797.

Stommel, H.M. (1961) Thermohaline convection with two stable regimes of flow. *Tellus*, **13**, 224–230.

Stone, P.H. and Miller, D.A. (1980) Empirical relations between seasonal changes in meridional temperature gradients and meridional fluxes of heat. *Journal of Atmospheric Science*, **37**, 1708–1721.

Stone, P.H. and Yao, M.S. (1990) Development of a two-dimensional zonally averaged statistical-dynamical model. Part III: The parameterization of the eddy fluxes of heat and moisture. *Journal of Climate*, **3**, 726–740.

Tang, B. and Weaver, A.J. (1995) Climate stability as deduced from an idealized coupled atmosphere-ocean model. *Climate Dynamics*, **11**, 141–150.

Vallis, G.K. (1982) A statistical-dynamical climate model with a simple hydrological cycle. *Tellus*, **34**, 211–227.

Watterson, I.G. and Dix, M.R. (1996) Influences on surface energy fluxes in simulated present and doubled CO_2 climates. *Climate Dynamics*, **12**, 359–370.

Weaver, A.J., Aura, S.M. and Myres, P. (1994) Interdecadal variability in an idealized model of the North Atlantic. *Journal of Geophysical Research*, **99**, 12423–12441.

Weaver, A.J. and Hughes, T.M.C. (1994) Rapid interglacial climate fluctuation driven by North Atlantic ocean circulation. *Nature*, **367**, 447–450.

Weisse, R., Mikolajewicz, U. and Maier-Reimer, E. (1994) Decadal variability of the North Atlantic in an ocean general circulation model. *Journal of Geophysical Research*, **99**, 12411–12421.

Willebrand, J. (1993) Forcing the ocean by heat and freshwater fluxes. In *Energy and Water Cycles in the Climate System*, NATO ASI Series. E. Raschke and D. Jacob (eds) pp. 215–233. Berlin, Heidelberg: Springer-Verlag.

Winguth, A.M.E., Duplessy, J.-C., Maier-Reimer, E. and Mikolajewicz, U. (1996) On the sensitivity of an OGCM to glacial boundary conditions. *Paleoceanography*, submitted.

Winton, M. (1997) The effect of cold climate upon North Atlantic Deep Water formation in a simple ocean-atmosphere model. *Journal of Climate*, **10**, 37–51.

Zhang, S., Greatbatch, R.J. and Lin, C.A. (1993) A reexamination of the polar halocline catastrophe and implications for coupled ocean-atmosphere modeling. *Journal of Physical Oceanography*, **23**, 287–299.

Zhang, S., Lin, C.A. and Greatbatch, R.J. (1995) A decadal oscillation due to coupling between an ocean circulation model and a thermodynamic sea-ice model. *Journal of Marine Research*, **53**, 79–106.

Meteorology, Hamburg, Report No. 15.

Oort, A.H. and Peixoto, J.P. (1983) Global angular momentum and energy balance requirements from observations. *Advances in Geophysics*, **25**, 355–490.

ERRATUM

Typo in equation (8):

Replace **0.72** by **0.072** in the equation of state!